NASA TM X-218

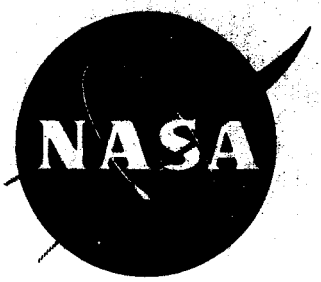

TECHNICAL MEMORANDUM

X-218

INTERFERENCE EFFECTS AT TRANSONIC SPEEDS OF JETS EXHAUSTING FROM THE HULL STEP OF A MODEL OF A LARGE, WATER-BASED AIRPLANE

By Beverly Z. Henry, Jr.

Langley Research Center
Langley Field, Va.

Declassified February 6, 1962

NATIONAL AERONAUTICS AND SPACE ADMINISTRATION
WASHINGTON

January 1960

NATIONAL AERONAUTICS AND SPACE ADMINISTRATION

TECHNICAL MEMORANDUM X-218

INTERFERENCE EFFECTS AT TRANSONIC SPEEDS OF JETS EXHAUSTING FROM THE HULL STEP OF A MODEL OF A LARGE, WATER-BASED AIRPLANE

By Beverly Z. Henry, Jr.

SUMMARY

An investigation has been conducted at transonic speeds to determine the interference effects of two sonic jets exhausting through the hull step of a model of a large, water-based airplane. The tests were conducted through the Mach number range from 0.6 to 1.10 at angles of attack from -2.1° to 6.6°. Hydrogen peroxide decomposition units were used for simulation of the jet exhausts and were operated at jet total-pressure ratios from no-flow to 7.3. Lift, drag, and pitching-moment coefficients as well as hull step and base-pressure coefficients were measured. The results indicated that for the range of this investigation the interference effects induced by jet operation were of a minor nature. Small increases in lift and a small, nose-up pitching moment occurred. The drag followed a conventional variation with increasing jet total-pressure ratio with only small overall effects noted. The configuration was statically stable throughout the investigation, and the stability was generally increased slightly by jet operation. Small positive changes in trim lift coefficient were induced by the jets.

INTRODUCTION

The investigation reported herein is part of a general research program to evaluate the characteristics of large, multiengine, water-based airplanes capable of flight at transonic and supersonic speeds. In the design of the particular configuration considered in this investigation, it was found that appreciable reductions in frontal area could be obtained by submerging two of the four engines in the flotation part of the hull forebody. This was accomplished by locating the

engines in such a manner that the jets exhausted through the hull step and below the hull afterbody. Such an installation was of interest from the standpoint of jet-interference effects. Previous work such as reported in references 1 and 2 indicated the possibility of favorable interference effects on lift. The relatively large projected area of the blunt hull step suggested possible adverse jet-interference effects on drag. (See, for example, ref. 3.)

The present investigation, designed to evaluate the interference effects of the two jets exhausting through the hull step, was conducted in the Langley 16-foot transonic tunnel at Mach numbers from 0.6 to 1.10, angles of attack from -2.1° to 6.6°, and jet total-pressure ratios from no flow to 7.3. Simulation of the jet exhausts was accomplished by using the hydrogen peroxide facilities of the Langley 16-foot transonic tunnel. L 5 8 7

The configuration had axial developments of cross-sectional area for a Mach number of 1.4, and the models tested were approximately 1/58 scale. Static aerodynamic characteristics (unpublished) have been determined in the Langley 8-foot transonic pressure tunnel, and the hydrodynamic characteristics are reported in reference 4.

SYMBOLS

The coefficients used in the following symbols are based on the stability system of axes:

A cross-sectional area, sq in.

C_L lift coefficient from balance measurements, including component of jet thrust, $\frac{\text{Lift}}{q_\infty S}$

C_D drag coefficient from balance measurements, including component of jet thrust, $\frac{\text{Drag}}{q_\infty S}$

C_m pitching-moment coefficient from balance measurements, including component of jet thrust, $\frac{\text{Pitching moment about } \bar{c}/4}{q_\infty S \bar{c}}$

$C_{L,j}$ lift coefficient with component of jet thrust removed

$C_{D,j}$	drag coefficient with component of jet thrust removed
$C_{m,j}$	pitching-moment coefficient with component of jet thrust removed
$\Delta C_{L,j}$	interference lift coefficient, $(C_{L,j})_{\text{jet on}} - (C_{L,j})_{\text{jet off}}$
$\Delta C_{D,j}$	interference drag coefficient, $(C_{D,j})_{\text{jet on}} - (C_{D,j})_{\text{jet off}}$
$\Delta C_{m,j}$	interference pitching-moment coefficient, $(C_{m,j})_{\text{jet on}} - (C_{m,j})_{\text{jet off}}$
$C_{D,i}$	duct internal-drag coefficient, $\frac{\text{Internal drag}}{q_\infty S}$
C_p	pressure coefficient, $\frac{p - p_\infty}{q_\infty}$
$\bar{c}$	wing mean aerodynamic chord (5.474 in. for these tests), in.
F	jet thrust, lb
$F_{i,c}$	ideal convergent nozzle thrust (assumes ideal weight flow, see fig. 5), lb
M	Mach number
m	mass-flow rate, lb/sec
m_i/m_∞	inlet mass-flow ratio
p	static pressure, lb/sq in.
p_t	total pressure, lb/sq in.
$p_{t,j}/p_\infty$	jet total-pressure ratio
q	dynamic pressure, $\frac{\gamma}{2}pM^2$, lb/sq in. or lb/sq ft
S	wing area (0.594 sq ft for these tests), sq ft
α	angle of attack (referenced to hull base line), deg

γ ratio of specific heats (1.4 for air, 1.27 for 90-percent hydrogen peroxide decomposition products)

Subscripts:

b fuselage base

j jet

∞ free stream

1,2 orifice designations

APPARATUS AND METHODS

Wind Tunnel and Models

The investigation reported herein was conducted in the Langley 16-foot transonic tunnel. The configuration investigated, shown in figures 1 and 2, employed four engines: two in the forward portion of the hull exhausting through the hull step and two mounted in a single nacelle well up on the vertical tail to avoid water ingestion during takeoff and landing. In the design of this configuration, it was assumed that taxi operations would be accomplished by using only the two rear engines while the forward engine exits remained sealed by watertight doors. For takeoff the configuration would be accelerated by the rear engines to the speed at which the hull step vented after which the doors could be opened and the forward engines started. A complete tabulation of physical characteristics of the full-scale configuration can be found in reference 4. The two rear engines were so located as to cause no unusual jet-interference effects and consequently were not equipped for jet simulation.

The two models used in the investigation differed only in the external shape of the body region near the nose. (See figs. 1 and 2.) One model (fig. 2(a)) duplicated the actual configuration in that it employed a single inlet in the forward portion of the hull to supply the two embedded engines. The scaled inlet and exits were connected by smooth ducts which allowed unobstructed flow through the inlet. The entire body was constructed of plastic. On the second model (fig. 2(b)), a solid nose replaced the inlet and was faired in a manner to give a smooth area transition. (See fig. 3.) The central portion of this body was of stainless steel and housed two hydrogen peroxide decomposition units for the simulation of jet exhausts. The small gap between the simulator nozzles and the body shell was sealed with a high-temperature, silicone-rubber compound to minimize leakage.

Turbojet Simulation

The two forward engines were simulated with hydrogen peroxide units mounted in the model as shown in figure 4. The two units were rigidly attached to the model and were supplied with hydrogen peroxide through a flexible coil which allowed model forces to deflect the balance. All balance outputs, therefore, contained the effects of jet thrust.

The turbojet-simulator units (fig. 5), which were of the type described in reference 5, used a silver-screen catalyst bed for the decomposition of 90-percent concentrated hydrogen peroxide (decomposition temperature approximately 1360° F) and exhausted the gas through a sonic nozzle scaled to represent a non-afterburning condition. External-body-size limitations dictated the internal shape of the nozzle-entrance section. Each unit was angled down 5° from the hull base line and out 1.25° from the plane of symmetry (fig. 4).

The measured performance of the simulator units is presented in figure 5. Experimental pressure ratios shown in this figure are average values for the two units. Although the measured thrust values were linear, they were somewhat lower than those normally encountered. (See, for example, ref. 5.) This low performance may be due in some measure to the small size of the units, but this cannot be verified. A trend in this direction may be noted in reference 5. Pressure measurements along the nozzle wall indicated that subsonic flow existed up to the sharply converging exit portion.

Tests

The models were tested with the power off for the Mach number range from 0.60 to 1.10 at angles of attack from approximately -2° to the angle corresponding to the maximum allowable load on the wing. Jet-on data were obtained only at Mach numbers of 0.8, 0.9, 1.0, and 1.10, but these data were considered to be sufficient to define the nature of any interference effects.

All tests were conducted with artificial transition fixed at 0.10c on the wing and horizontal tail and at the inlet stations. Transition was accomplished by using No. 120 carborundum grains applied in bands 0.1 inch wide at each point. The Reynolds number, based on $\bar{c} = 5.474$ inches, varied from 1.45×10^6 to 1.76×10^6.

With the jets on, some effect of temperature was noted in the balance output. In order to minimize this effect, the simulator-equipped model was tested through the Mach number and angle-of-attack ranges with the jets off to obtain an accurate datum. During jet-on

tests, frequent jet-off points were taken and the increments (jet-on minus jet-off) thus obtained were applied to the jet-off data to obtain jet effects.

Measurements

Normal force, axial force, and pitching moment were measured by a strain-gage-type balance. As previously noted each of the component outputs contained the effects of jet thrust. Body base pressures, step pressures, and jet total-pressure ratios were measured by means of electrical pressure transducers. Jet-simulator thrust was obtained from static measurements adjusted to existing free-stream conditions.

Data Reduction

All balance and pressure-transducer outputs were fed directly to digitizing equipment and then to an automatic card punch. The data were then reduced to coefficient form by automatic computing equipment.

The drag values have been corrected for the effects of internal flow through the forward inlet and ducting where applicable. The magnitude of these corrections is indicated in figure 6. No corrections for the flow through the rear nacelle have been applied inasmuch as this nacelle was used for both configurations tested.

RESULTS AND DISCUSSION

Configuration Comparison

A comparison of the measured forces and moments (jet-off) for the inlet model with those for the jet-simulator model is made in figure 7(a). Within the range of the present tests, only slight differences were noted. A comparison of jet-off hull base and step pressures for the two models is made in figures 7(b) and 7(c). The base pressure coefficients are in good agreement although the step pressures show more discrepancy. Although exact duplication of the two configurations was attempted in the immediate region of the jet exits, it should be noted that certain small differences could not be avoided. These differences resulted in small changes in orifice location which may account for the discrepancies in measured pressures.

From these results the jet-interference effects obtained by using the jet-simulator model may be assumed to be a reasonable indication

of similar effects on the inlet model. Therefore, all subsequent discussion will be devoted to results obtained from the jet-simulator-equipped model.

Jet Effect on Lift Coefficient

The variation of lift coefficient with jet total-pressure ratio for several constant values of Mach number and angle of attack is shown in figure 8(a). These data contain the lift component of the thrust vector. This component is, however, of insignificant magnitude.

These results indicate that for all the conditions investigated the lift interference is quite small. It is in all cases, however, favorable with the favorable effect apparently increasing with Mach number, especially for $M_\infty > 1.0$. Previous investigations such as those of references 1 and 2 have indicated such a favorable interference; however, the low magnitude measured for this configuration was not unexpected. The interference would be expected to be felt primarily on the underside of the afterbody for a short distance downstream of the jet exits. This area is quite small compared to the total lifting surface and also serves as an effective barrier in preventing the interference effects from being felt by the wing. Incremental values of lift coefficient due to the jet are shown at an enlarged scale in figure 8(b).

No visual representations of the flow were obtained. As a matter of interest, the jet boundary was estimated for a pressure ratio of 7 (maximum for these tests was 7.3) by using the data of reference 5. This boundary is depicted in figure 9 and indicates that the jet did not impinge on the model surfaces. Lack of any evidence of overheating on the body surfaces in the vicinity of the jet exits tended to confirm this indication.

Jet Effect on Drag Coefficient

The variation of drag coefficient with jet pressure ratio at constant values of Mach number and angle of attack is shown in figure 10. The data of figure 10(a) include the drag component of the jet thrust and, in general, exhibit similar trends at all angles of attack and Mach numbers. The linear nature of the curves results from an overriding influence of the jet thrust which tends to conceal any interference effects which might be present.

The interference effects of the jet can be seen in figure 10(b) in which the thrust component has been removed from the data of figure 10(a). Here again, the influence of the jet is small but exhibits a characteristic variation of drag with pressure ratio; that is, with increasing

pressure ratio, the drag first decreases and then increases until the jet boundary has expanded sufficiently for interference with the external stream to occur at which point the drag would be expected to decrease once again. The curves have been arbitrarily faired between the no-flow point and a pressure ratio of 2 since no intermediate data were obtained. The point of favorable interference with the external stream was not reached in these tests with the possible exception of the data at $M_\infty = 1.10$. Incremental values of drag coefficient due to the jet are shown in figure 10(c).

It can be seen from the estimated jet boundary previously mentioned that any interference with the external stream would be restricted to a relatively small region at either side of the exit. (See fig. 9.) Hence, there is a possible explanation for lack of any favorable interference at the higher pressure ratios.

There is a large reduction in hull cross-sectional area from a point just ahead of the exit station to a point just aft of this station. (See fig. 3.) This reduction is of the order of one-third the total area with the jet exits occupying only about 17 percent of this area decrement. Effective-base-area relationships of these magnitudes on less complicated shapes would tend to indicate rather large adverse jet effects (ref. 3). Examination of the variation of hull step pressures with pressure ratio (fig. 11) indicates considerable aspiration in the approximate plane of the exits above a pressure ratio of 2. A configuration such as the present one with an area change of this magnitude diffused over a relatively large distance could, however, be expected to be less subject to severe jet effects than one in which the area change is abrupt. It is also evident from the area diagram that a favorable surface presents itself downstream from the exits for increased pressures from the jet. All of these factors apparently act as mitigating influences which tend to reduce the jet-interference effects to small values.

Jet Effect on Pitching-Moment Coefficient

The pitching-moment coefficient became more positive with increasing jet pressure ratio as shown in figure 12. A portion of this increase was due to a positive moment exerted by the jet thrust. (See fig. 1.) In figure 12(b) the moment due to thrust has been removed to indicate jet-interference effects. This interference generally resulted in a nose-up pitching moment. Since it has been shown previously that the lift increments were quite small, it may be assumed that the interference effects are felt very near the jet exits. The exit plane is approximately 10 jet diameters forward of the model center of gravity. With all four engines operating, the rear engine thrust would create a moment tending to oppose that from the forward engines. With equal thrust on all engines there would remain a small nose-up pitching moment.

All of these factors emphasize the minor nature of the jet-interference effects due to the two forward engines. The incremental effects are plotted in figure 12(c).

Jet Effects on Stability

The variation of pitching-moment coefficient with lift coefficient is shown in figures 13(a) and 13(b) for the results with and without the components due to jet thrust, respectively. The static longitudinal stability for the configuration is shown in figure 14 for $\alpha \approx 0^{\circ}$. The configuration was stable throughout the range of these tests with maximum stability indicated near a Mach number of 1.0. Increasing jet pressure ratio generally resulted in an increase in stability with a maximum increase noted near $M_{\infty} = 1.0$. There is some indication, however, that at speeds higher than those tested here the jets might have a destabilizing effect. Similar trends were noted whether the moment due to thrust was included or not.

Trim lift coefficient (fig. 15) was made more positive by the jet interference. Minimum trim lift coefficient occurred near $M_{\infty} = 0.98$ with the change being less than 0.1 in all cases.

Since very little change in $\partial C_m/\partial C_L$ resulted from the removal of the thrust effect of the forward engines, it appears likely that operation of the rear engines would have little or no effect on static stability. A more negative value of trim lift coefficient might be expected however.

CONCLUDING REMARKS

An investigation has been made at transonic speeds to determine the interference effects of two sonic jets exhausting through the hull step of a model of a large water-based airplane. The results indicated that for the range of this investigation the interference effects were of a minor nature. Small increases in lift and a small, nose-up pitching moment occurred. These effects tended to increase with Mach number. Drag coefficient followed a conventional variation with increasing jet total-pressure ratio with only small overall effects noted. The configuration was statically stable throughout the investigation and this stability was generally increased slightly by operation of the jets. Small, positive changes in trim-lift coefficient were induced by the jets.

Langley Research Center,
National Aeronautics and Space Administration,
Langley Field, Va., October 9, 1959.

REFERENCES

1. Wasserbauer, Joseph F., and Englert, Gerald W.: Interaction of an Exhaust Jet and Elementary Contoured Surfaces Located in a Supersonic Air Stream. NACA RM E56A16, 1956.

2. Falanga, Ralph A., and Judd, Joseph H.: Flight Investigation of the Effect of Underwing Propulsive Jets on the Lift, Drag, and Longitudinal Stability of a Delta-Wing Configuration at Mach Numbers From 1.23 to 1.62. NACA RM L55I13, 1955.

3. Henry, Beverly Z., Jr., and Cahn, Maurice S.: Additional Results of an Investigation at Transonic Speeds To Determine the Effects of a Heated Propulsive Jet on the Drag Characteristics of a Series of Related Afterbodies. NACA RM L56G12, 1956.

4. Blanchard, Ulysse J.: Hydrodynamic Investigation of a Model of a Supersonic Multijet Water-Based Aircraft With Engines Exhausting From the Step. NACA RM L57F20, 1957.

5. Runckel, Jack F., and Swihart, John M.: A Hydrogen Peroxide Hot-Jet Simulator for Wind-Tunnel Tests of Turbojet-Exit Models. NASA MEMO 1-10-59L, 1959.

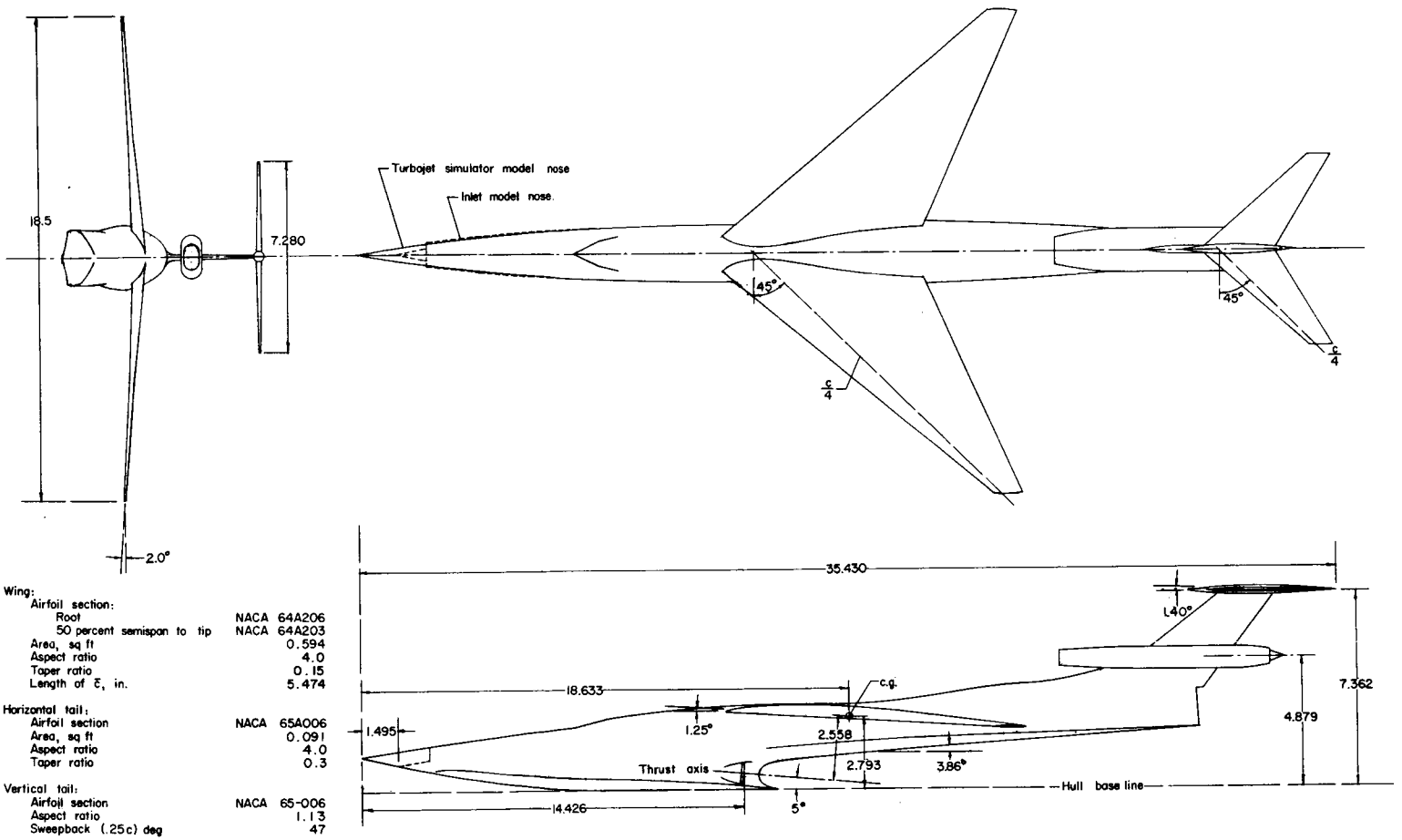

Wing:	
Airfoil section:	
Root	NACA 64A206
50 percent semispan to tip	NACA 64A203
Area, sq ft	0.594
Aspect ratio	4.0
Taper ratio	0.15
Length of $\bar{c}$, in.	5.474
Horizontal tail:	
Airfoil section	NACA 65A006
Area, sq ft	0.091
Aspect ratio	4.0
Taper ratio	0.3
Vertical tail:	
Airfoil section	NACA 65-006
Aspect ratio	1.13
Sweepback (.25c) deg	47

Figure 1.- Sketch of model configurations tested. All dimensions are in inches.

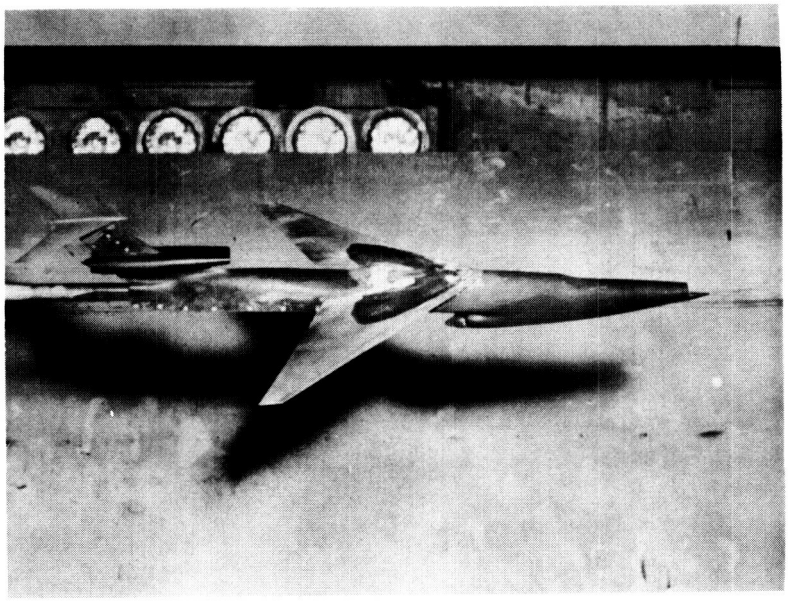

L-58-726a

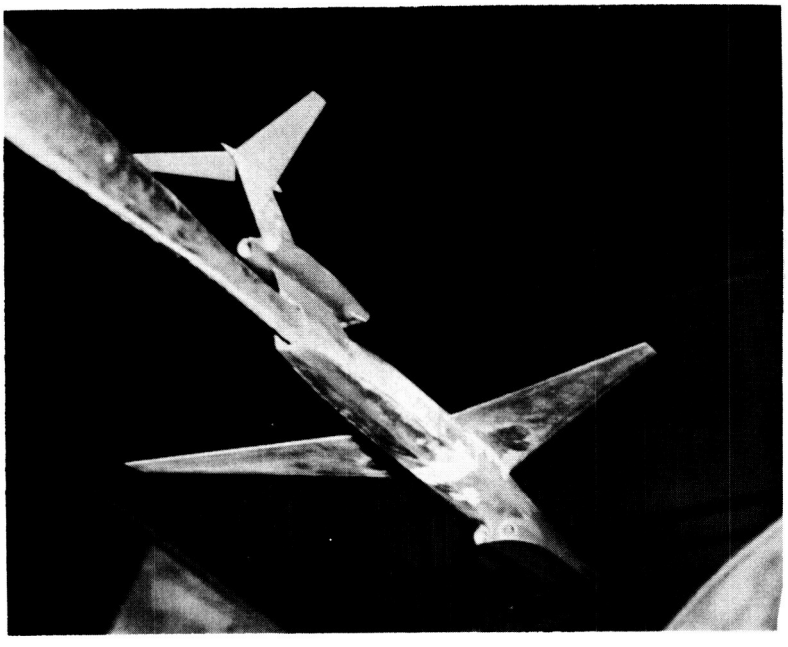

(a) Inlet model. L-58-725a

Figure 2.- Photographs of the models used in the investigation.

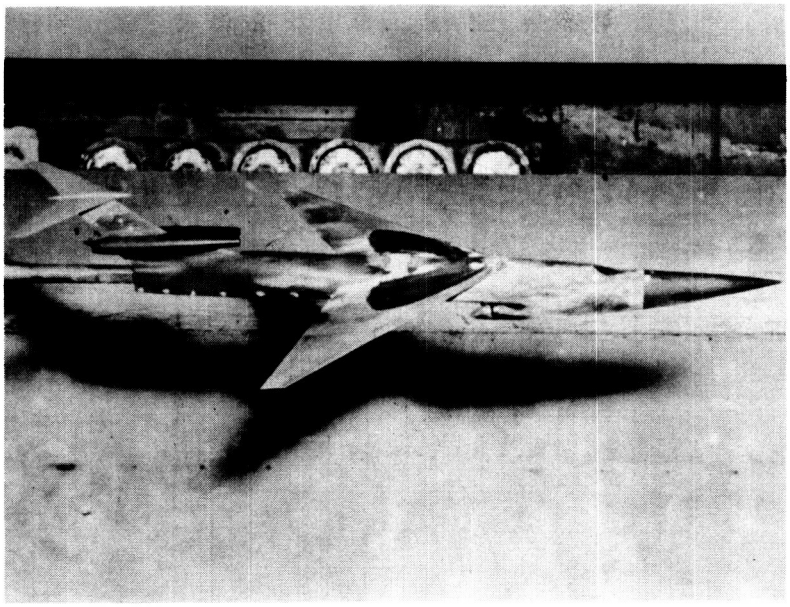

L-58-719a

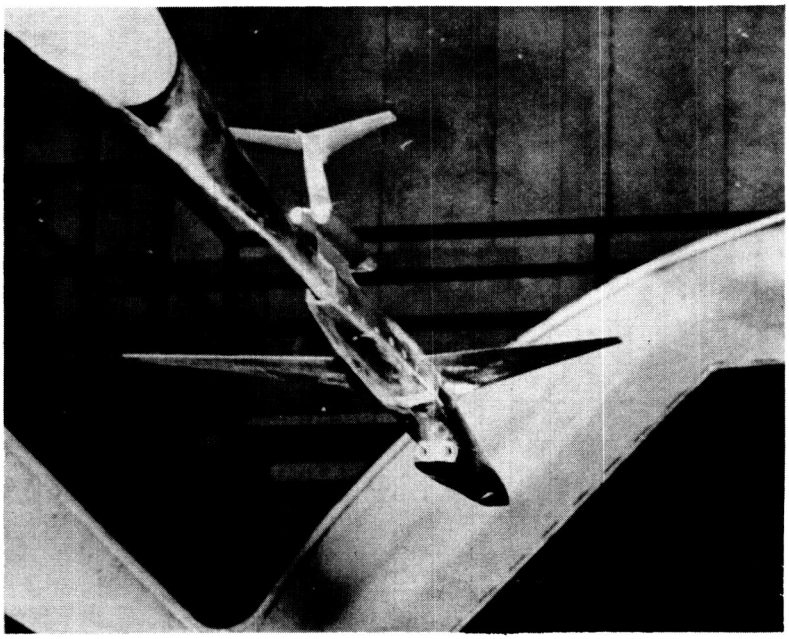

(b) Jet-simulator model. L-58-720a

Figure 2.- Concluded.

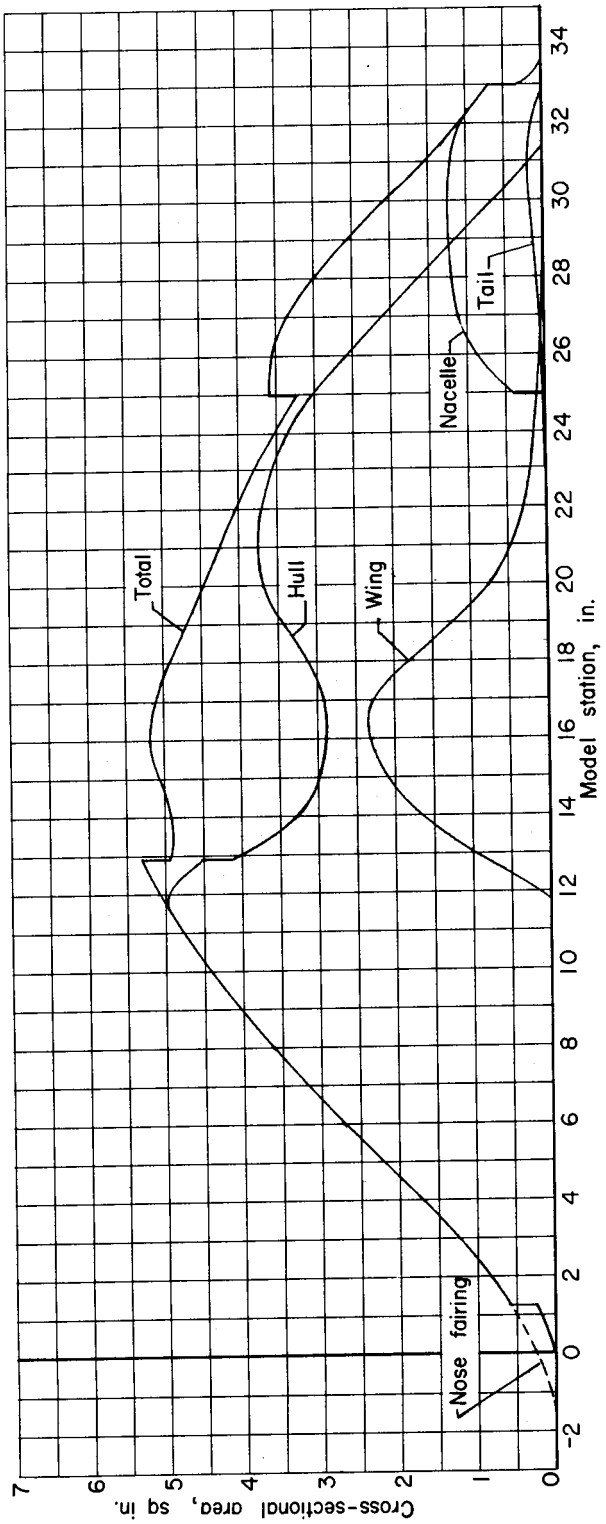

Figure 3.- Cross-sectional area distribution.

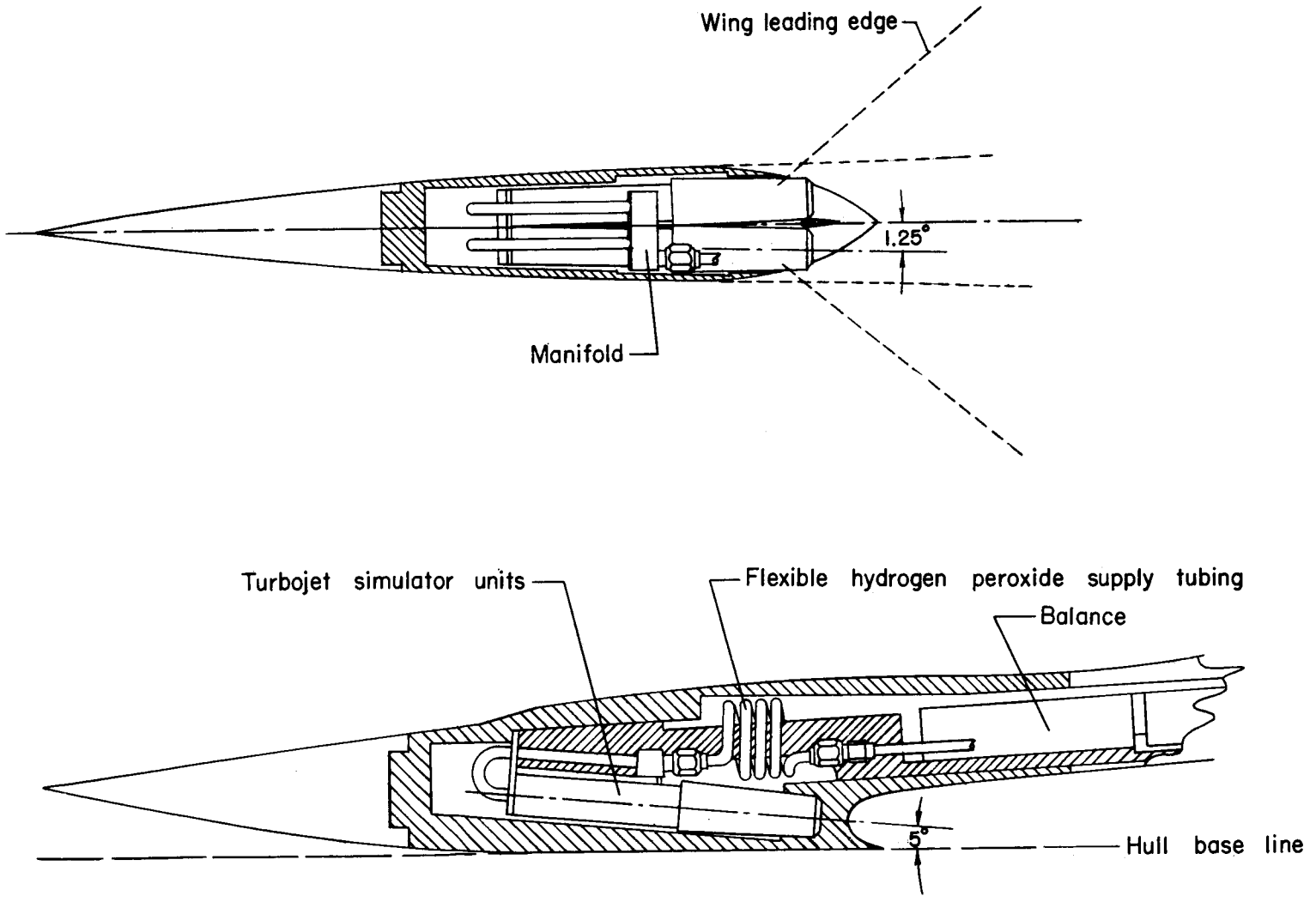

Figure 4.- Installation of the jet-simulator units in the model. All dimensions are in inches.

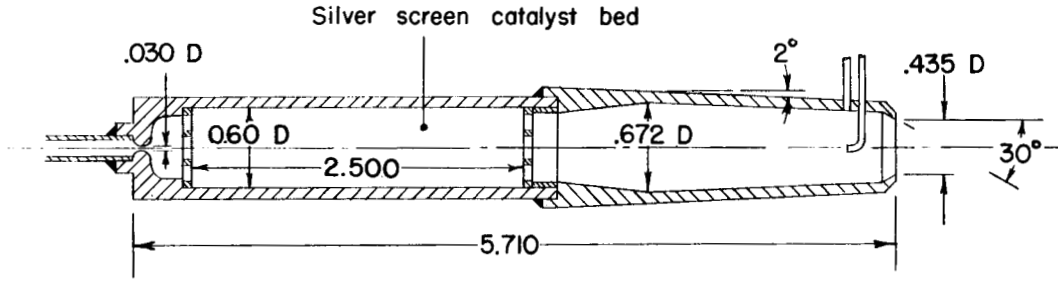

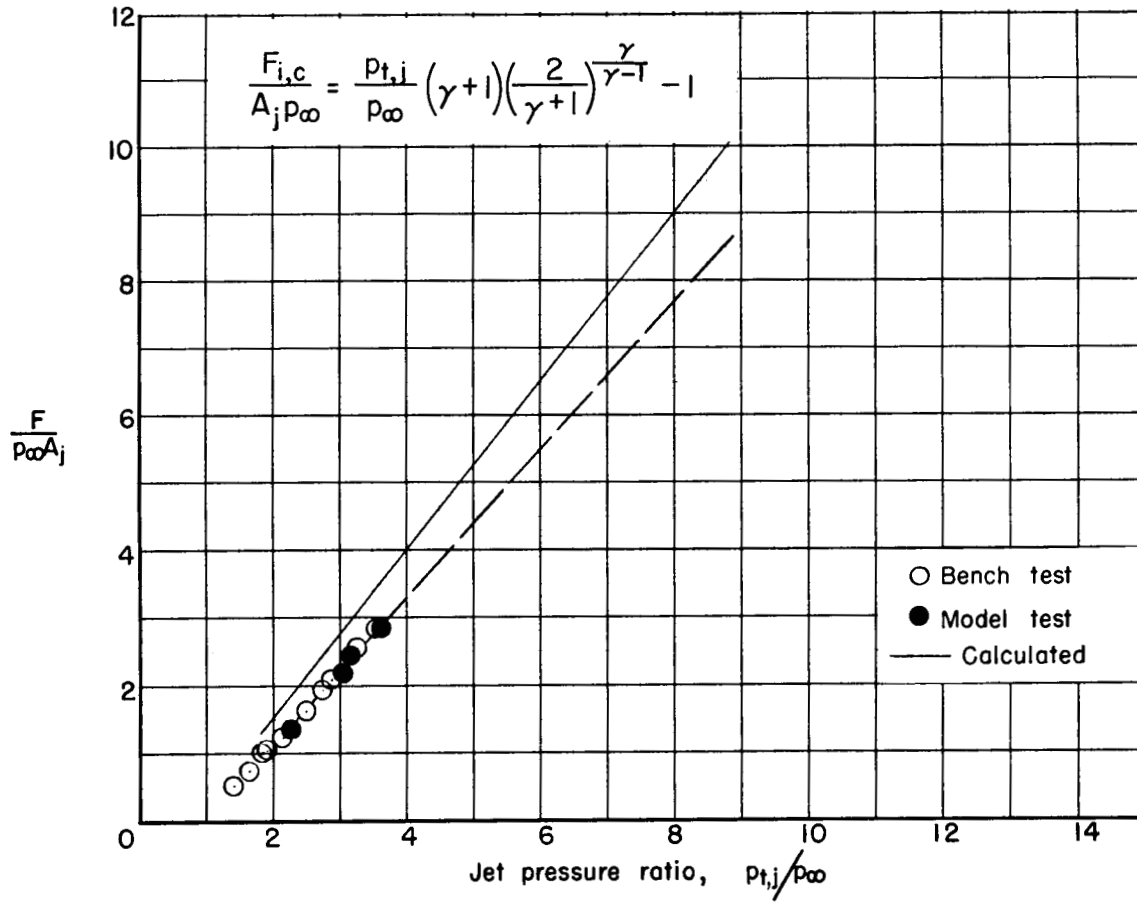

Figure 5.- Turbojet-simulator performance and physical details. All dimensions are in inches.

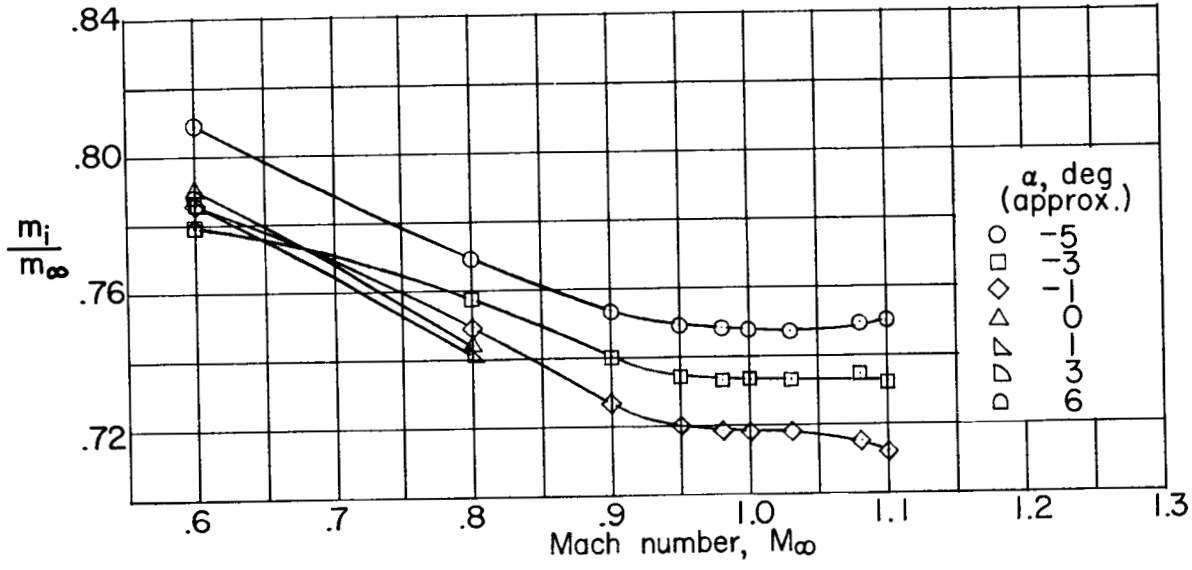

(a) Mass-flow ratio.

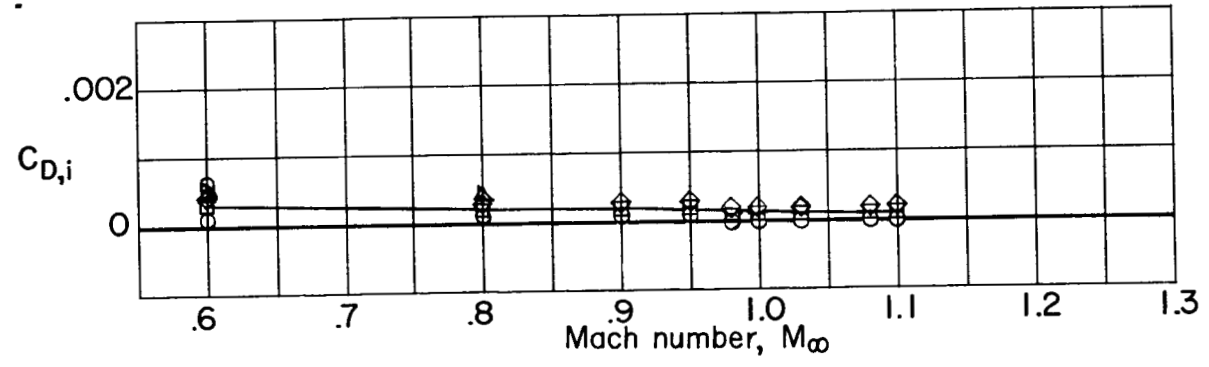

(b) Internal-drag coefficient.

Figure 6.- Internal-flow characteristics of the forward inlet and ducting of the inlet model.

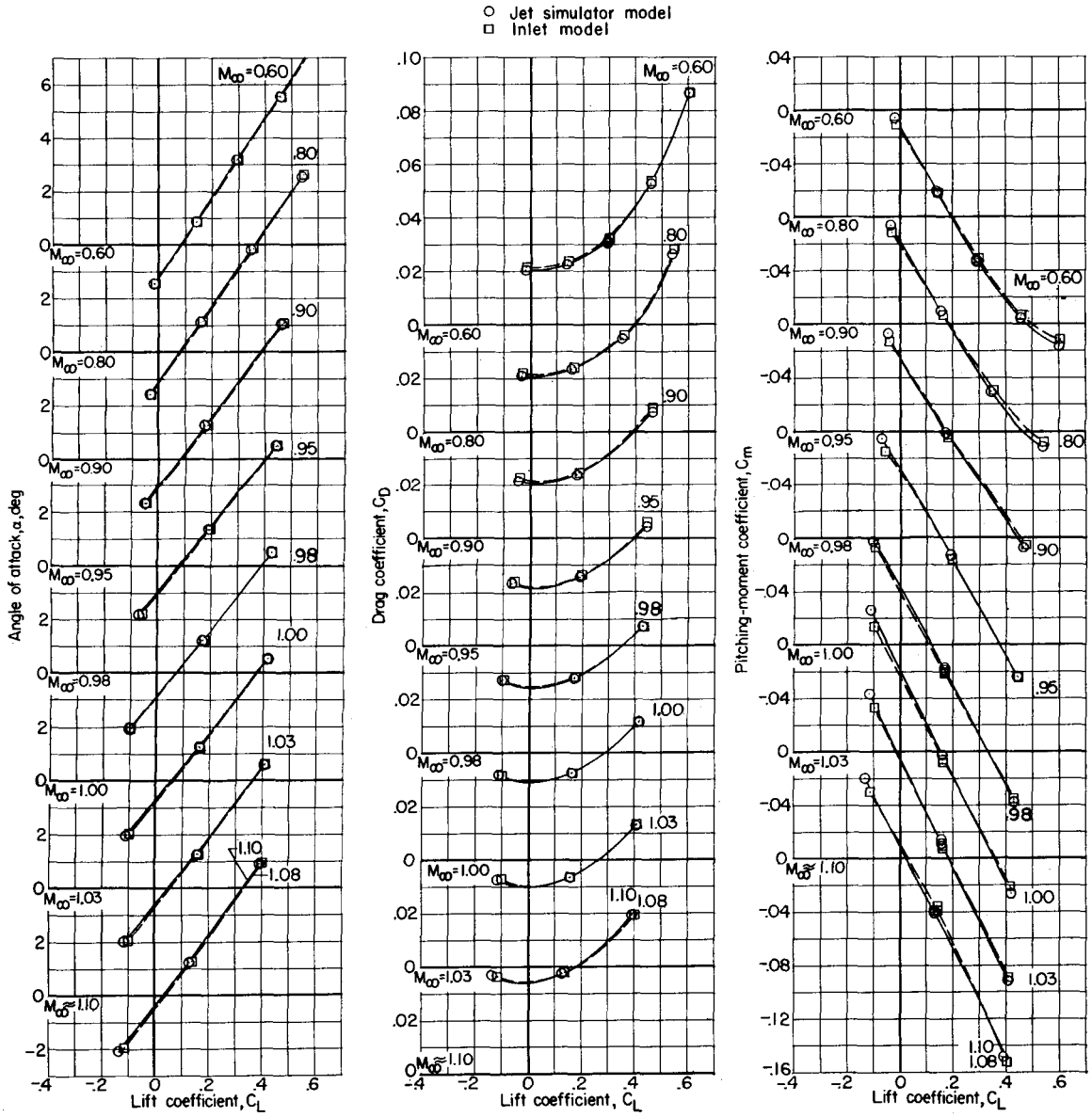

(a) Aerodynamic characteristics.

Figure 7.- Comparison of the inlet model and the turbojet-simulator-equipped model. No jet flow.

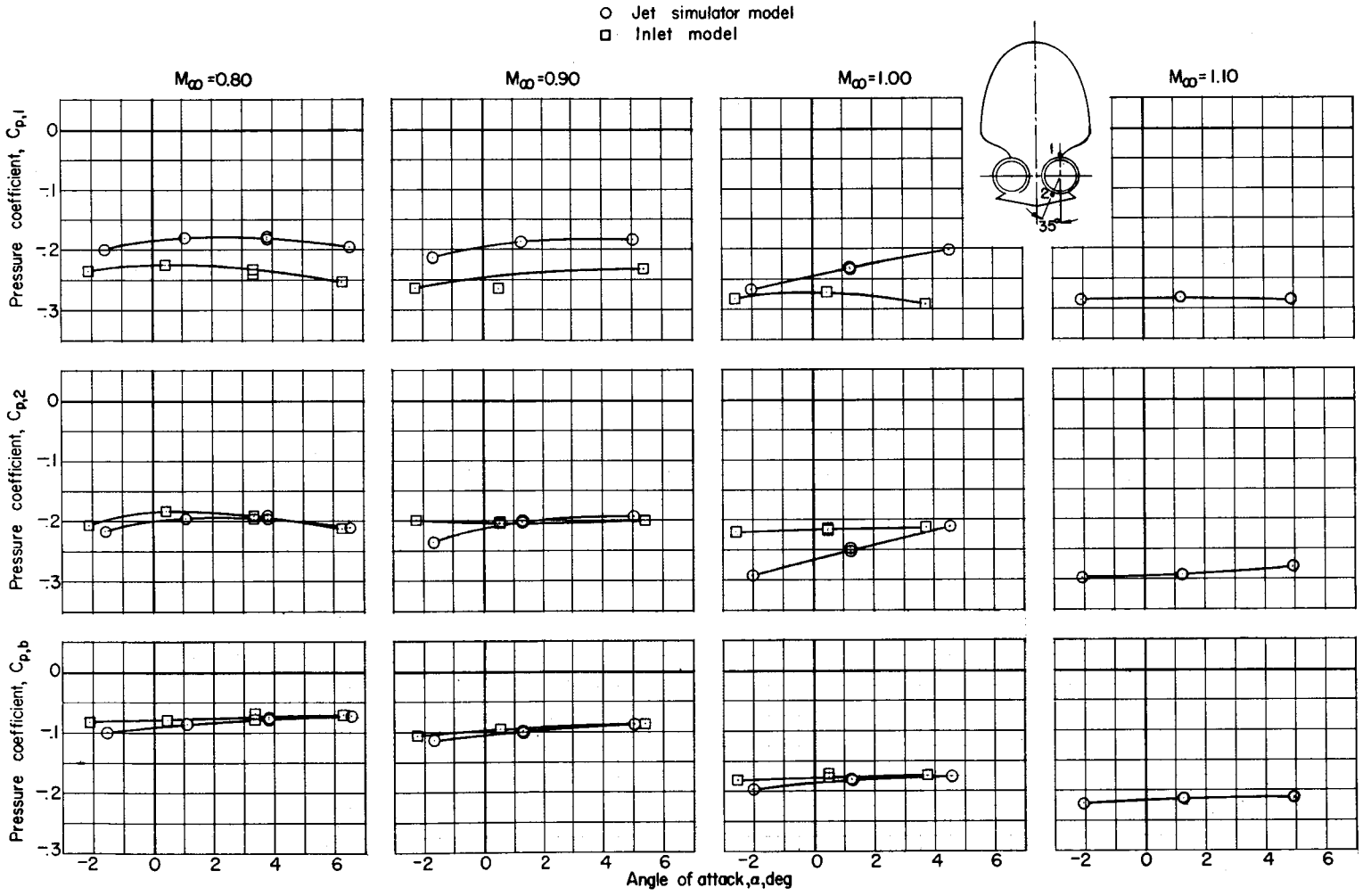

(b) Hull step and base pressure coefficients.

Figure 7.- Continued.

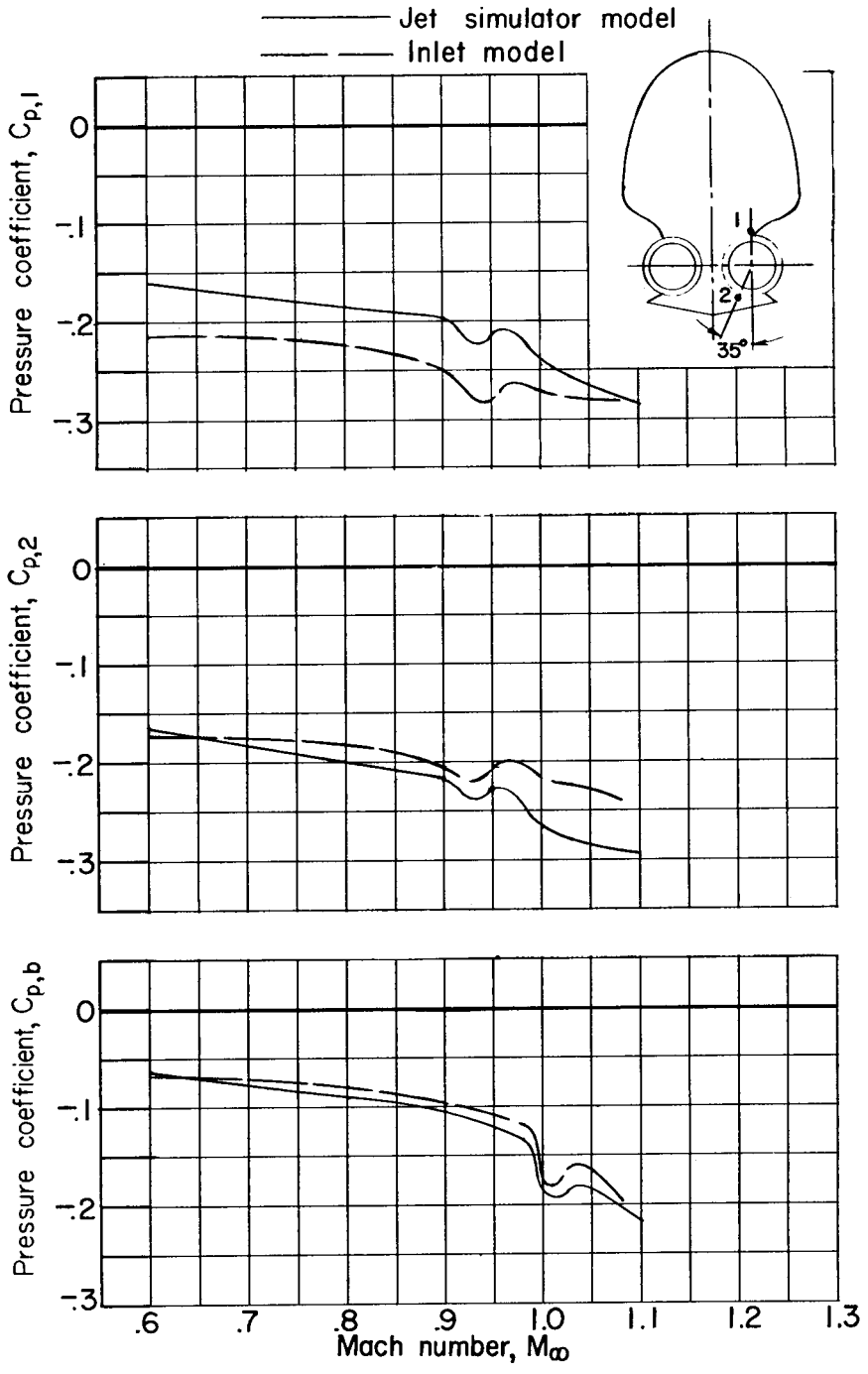

(c) Hull step and base pressure coefficients. $\alpha = 0^\circ$.

Figure 7.- Concluded.

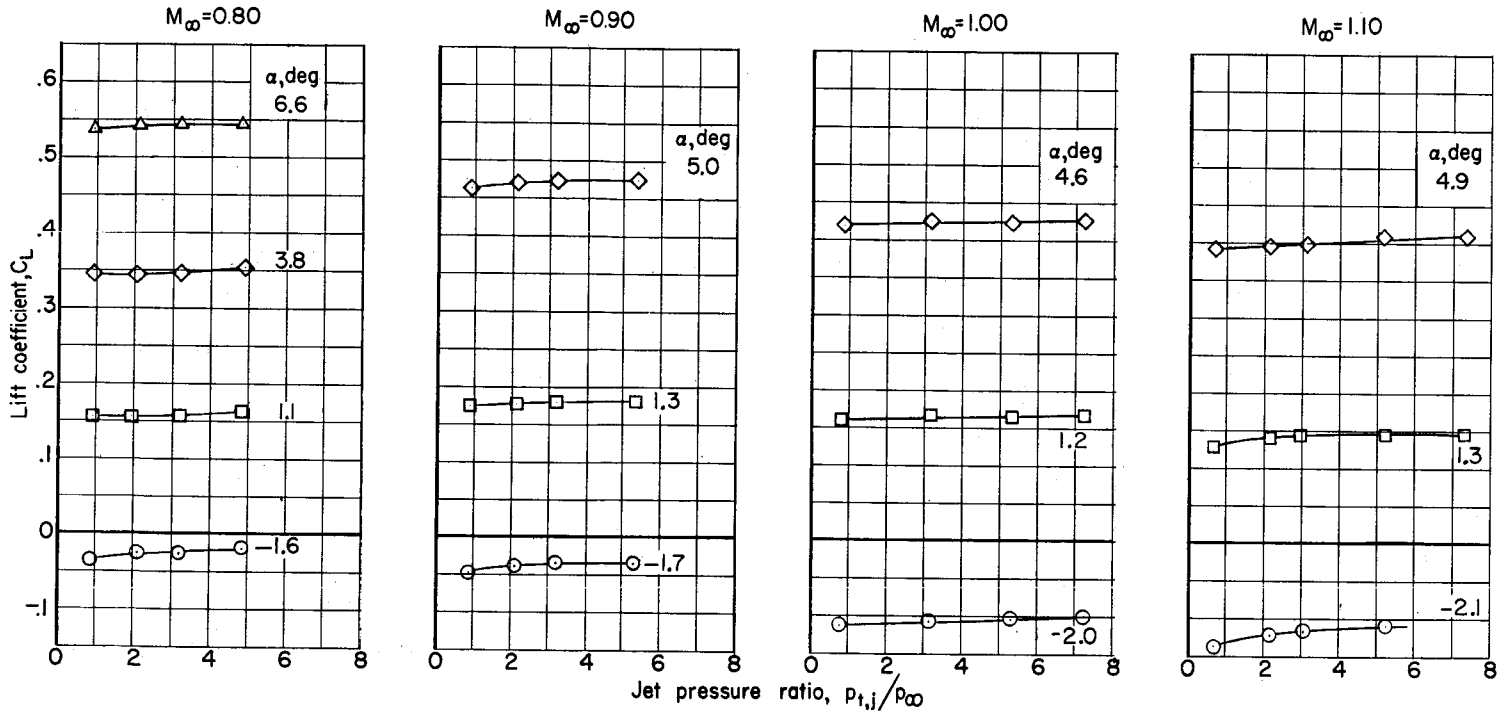

(a) Lift-coefficient (including component of jet thrust) variation with jet total-pressure ratio.

Figure 8.- Effects of jet interference on lift coefficient.

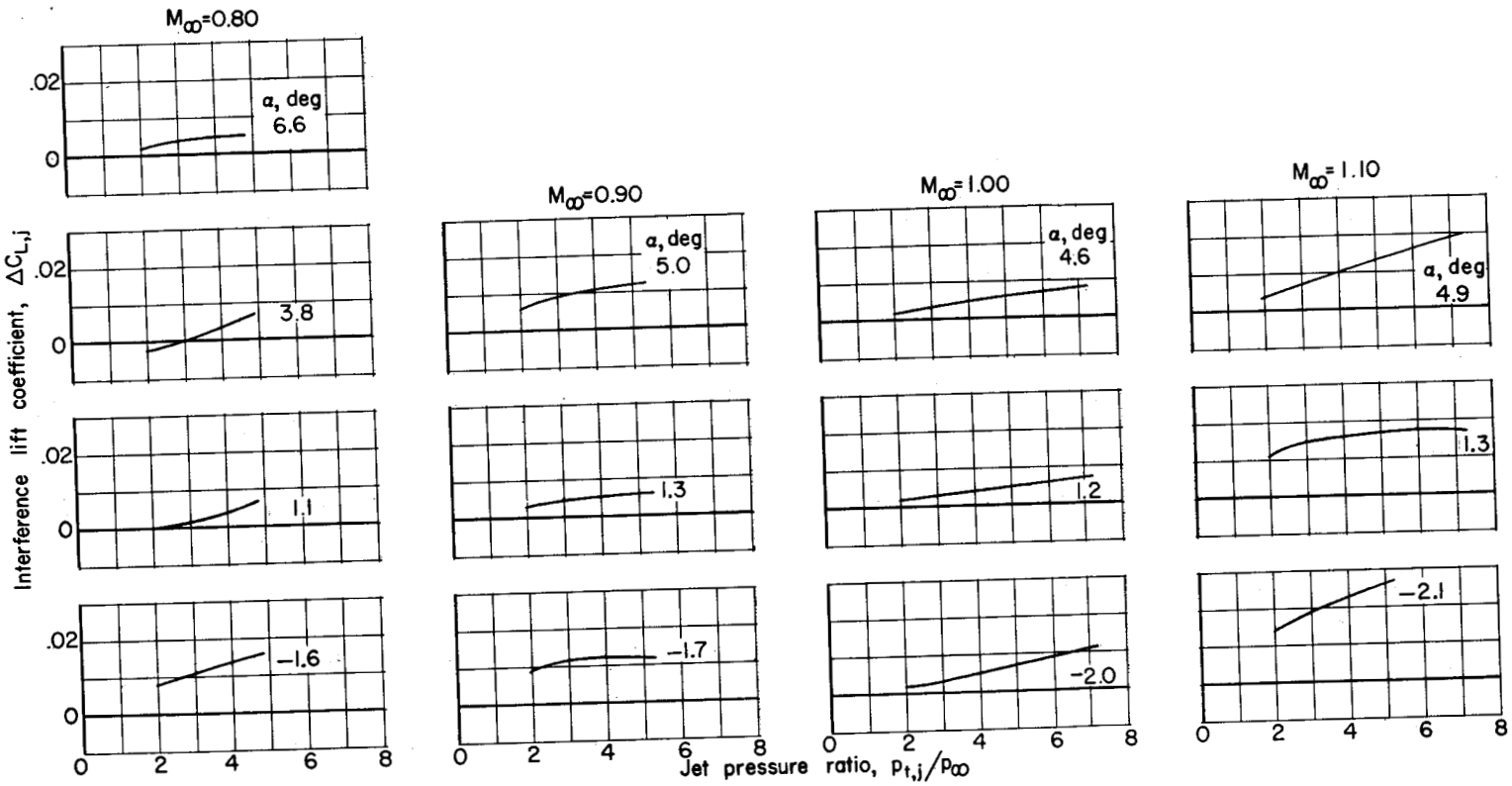

(b) Incremental lift coefficient due to jet interference.

Figure 8.- Concluded.

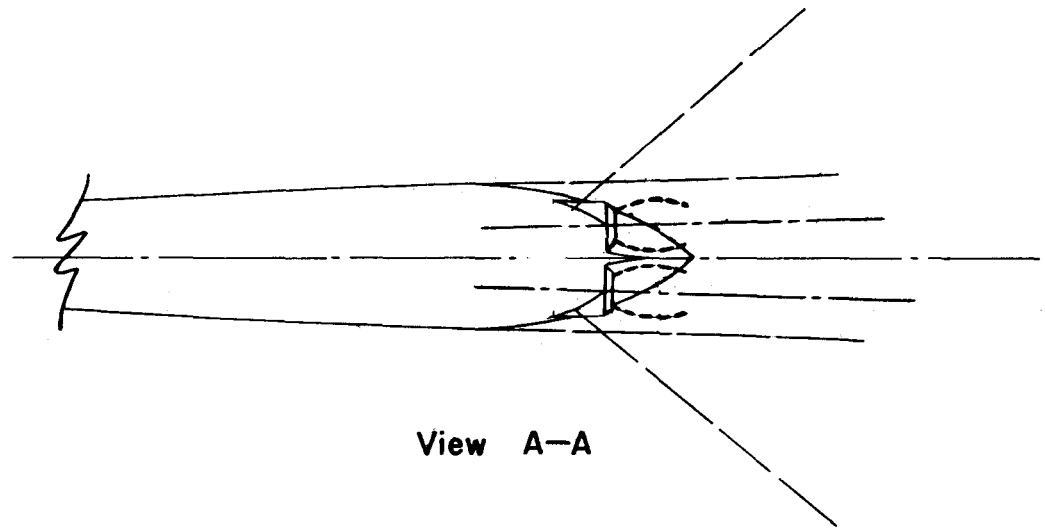

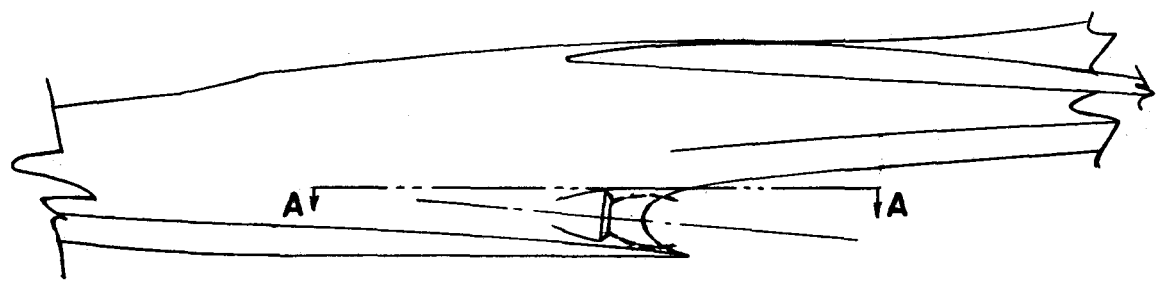

Figure 9.- Estimated jet boundary using the data of reference 5.
$p_{t,j}/p_{\infty} = 7$.

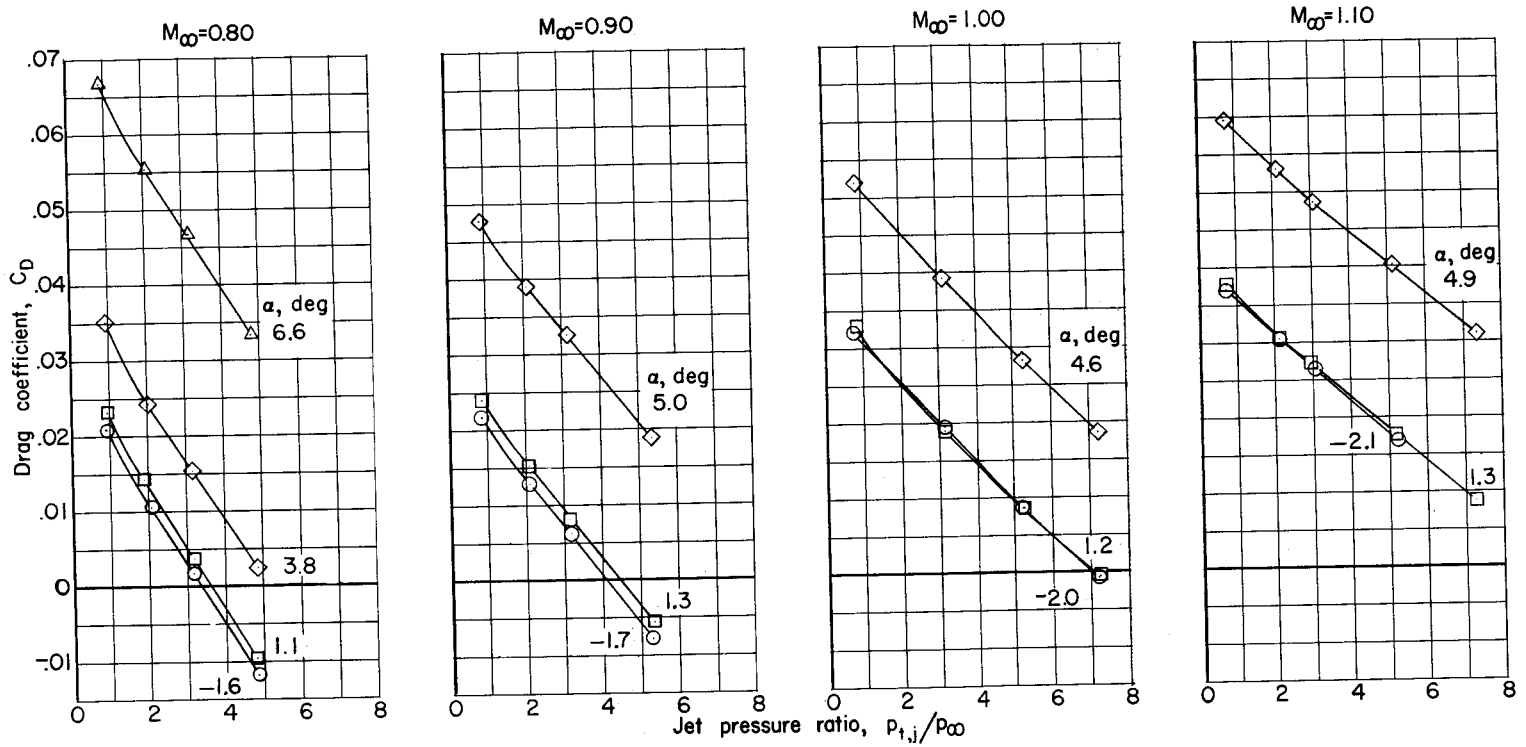

(a) Drag-coefficient (including component of jet thrust) variation with jet total-pressure ratio.

Figure 10.- Effects of jet interference on drag coefficient.

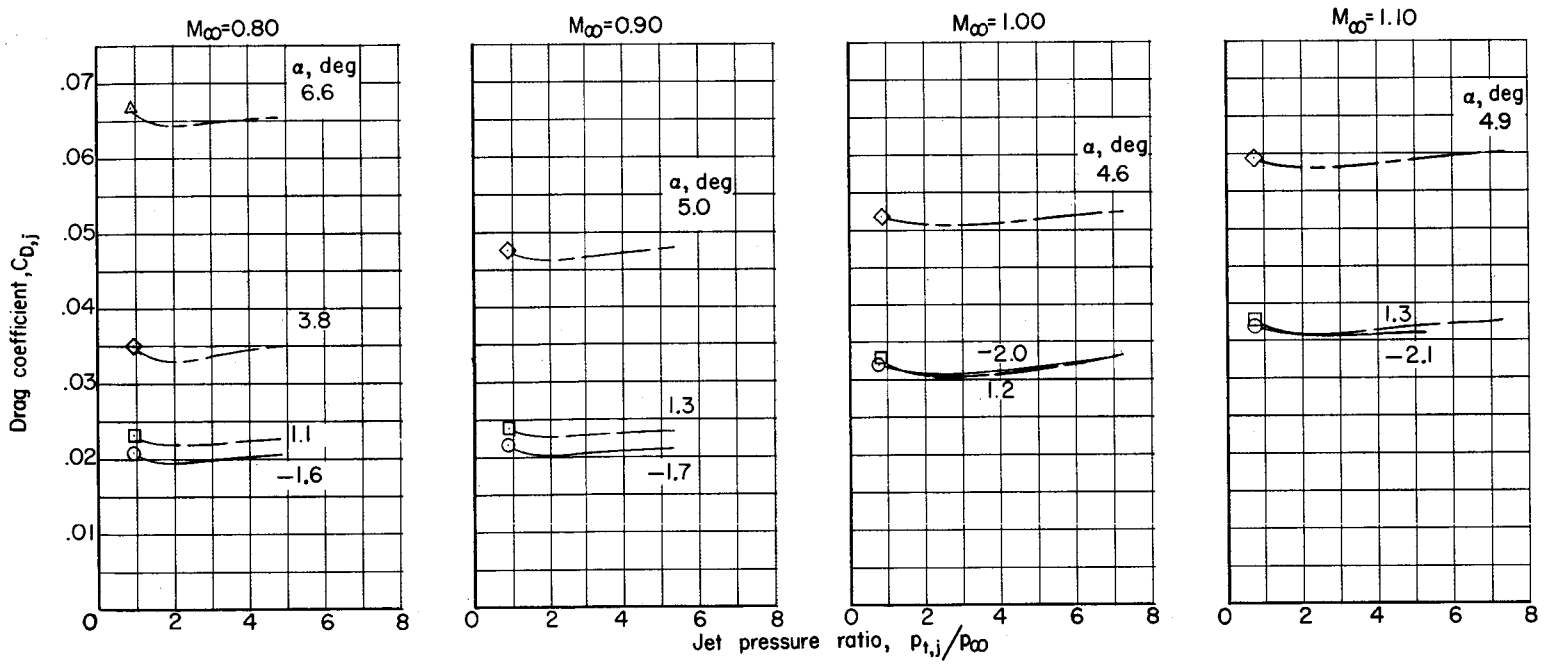

(b) Drag-coefficient (component of jet thrust removed) variation with jet total-pressure ratio.

Figure 10.- Continued.

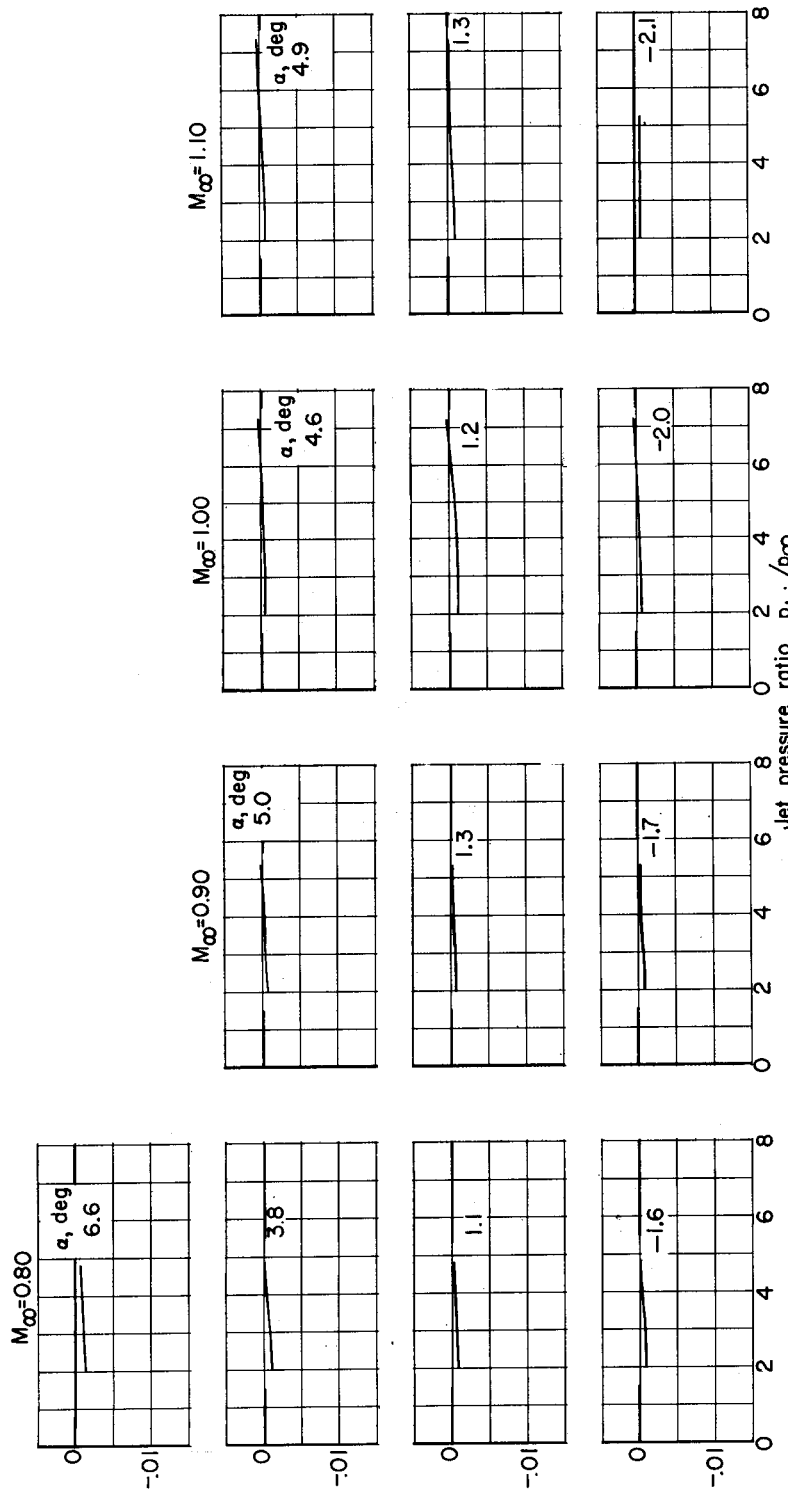

(c) Incremental drag coefficient due to jet interference.

Figure 10.- Concluded.

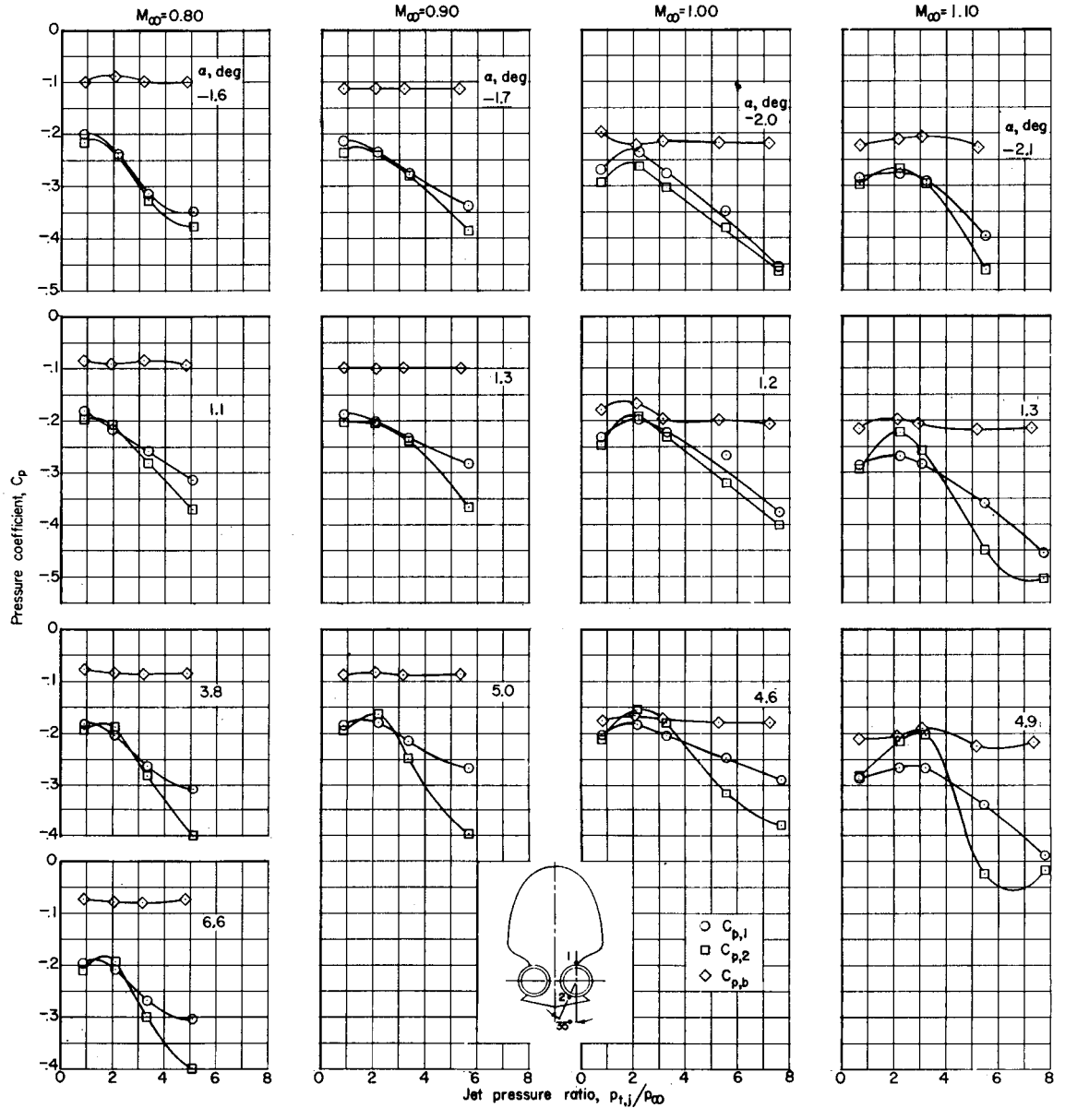

Figure 11.- Jet effects on hull step and base pressure coefficients.

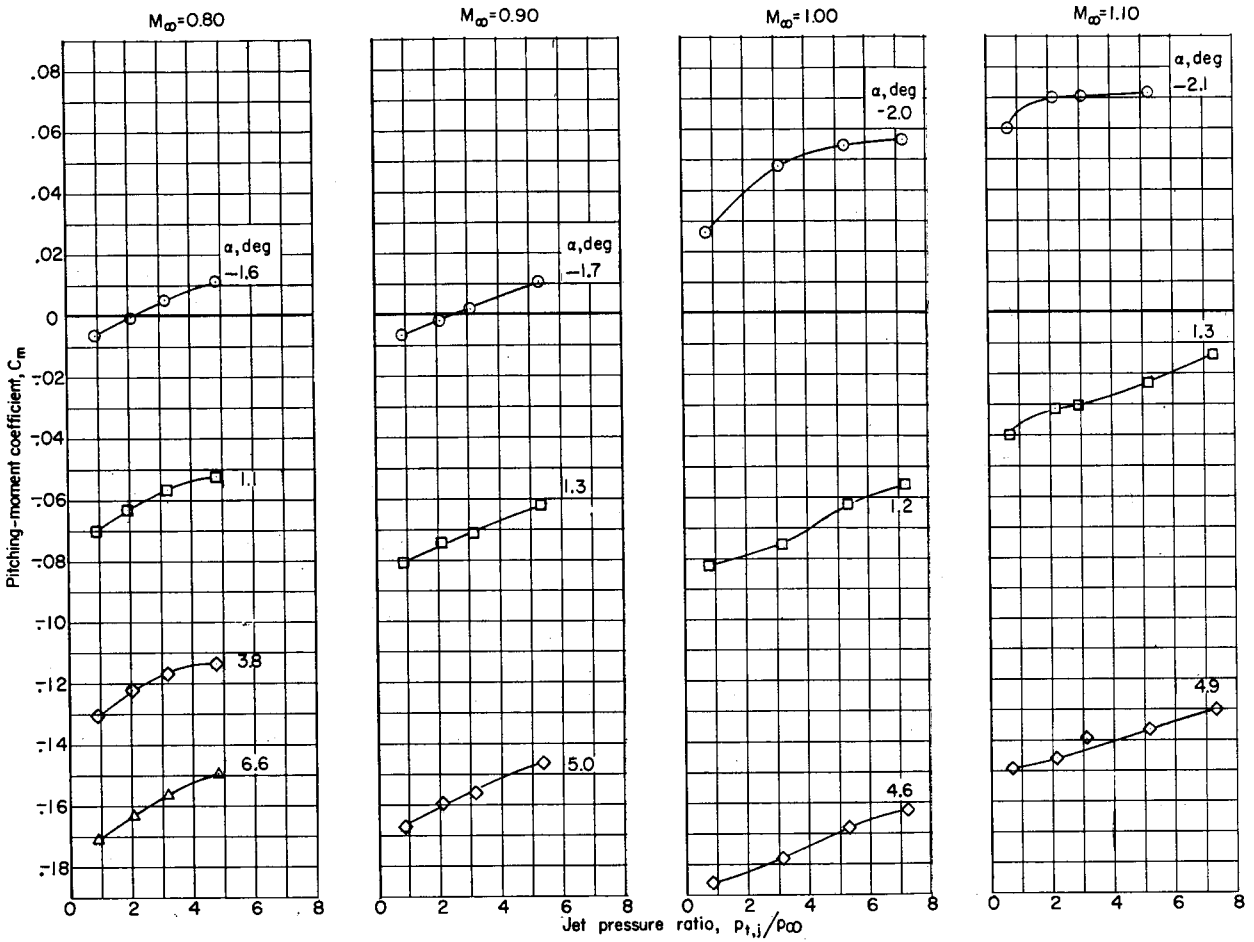

(a) Pitching-moment-coefficient (including moment due to jet thrust) variation with jet total-pressure ratio.

Figure 12.- Effects of jet interference on pitching-moment coefficient.

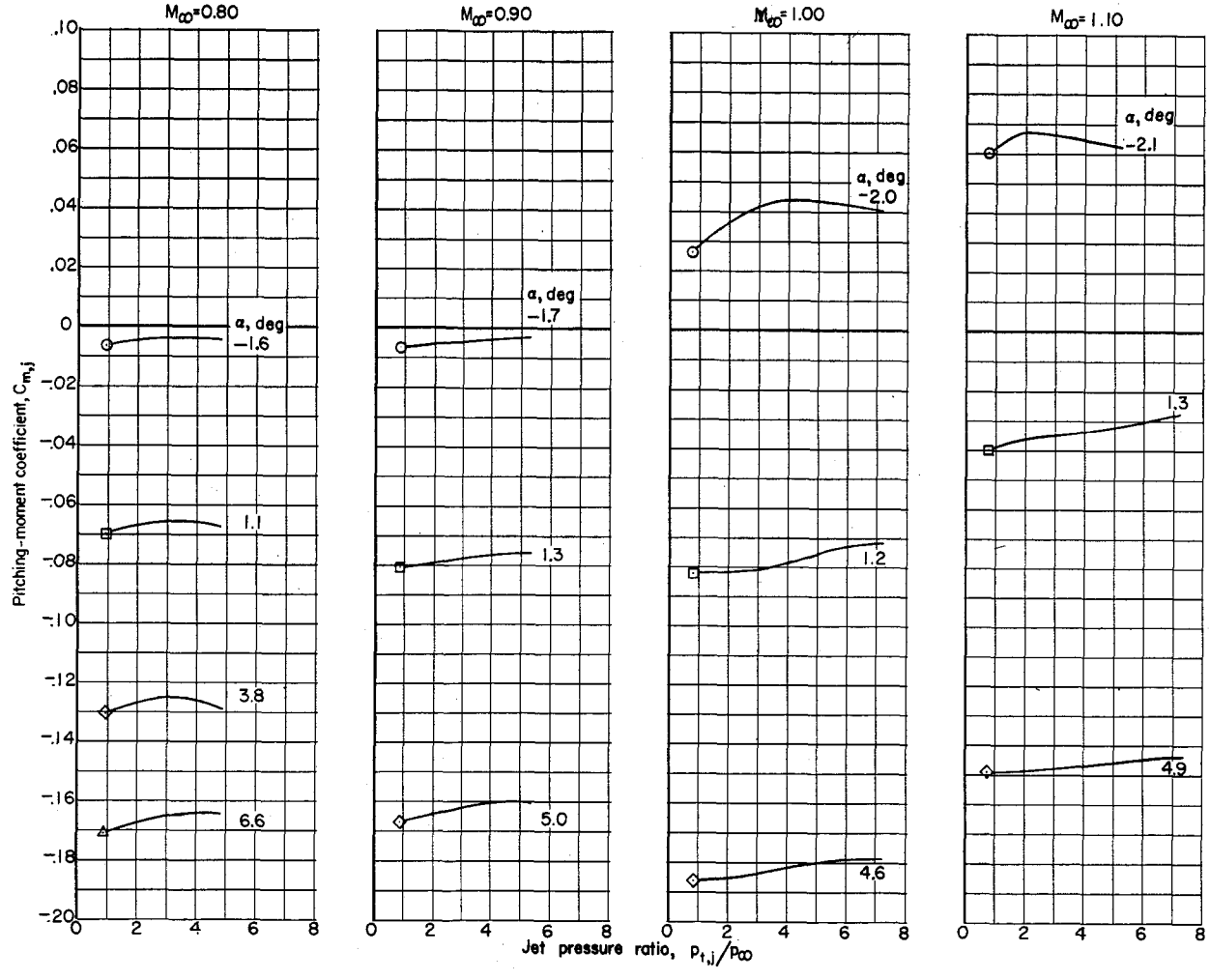

(b) Pitching-moment-coefficient (moment due to jet thrust removed) variation with jet total-pressure ratio.

Figure 12.- Continued.

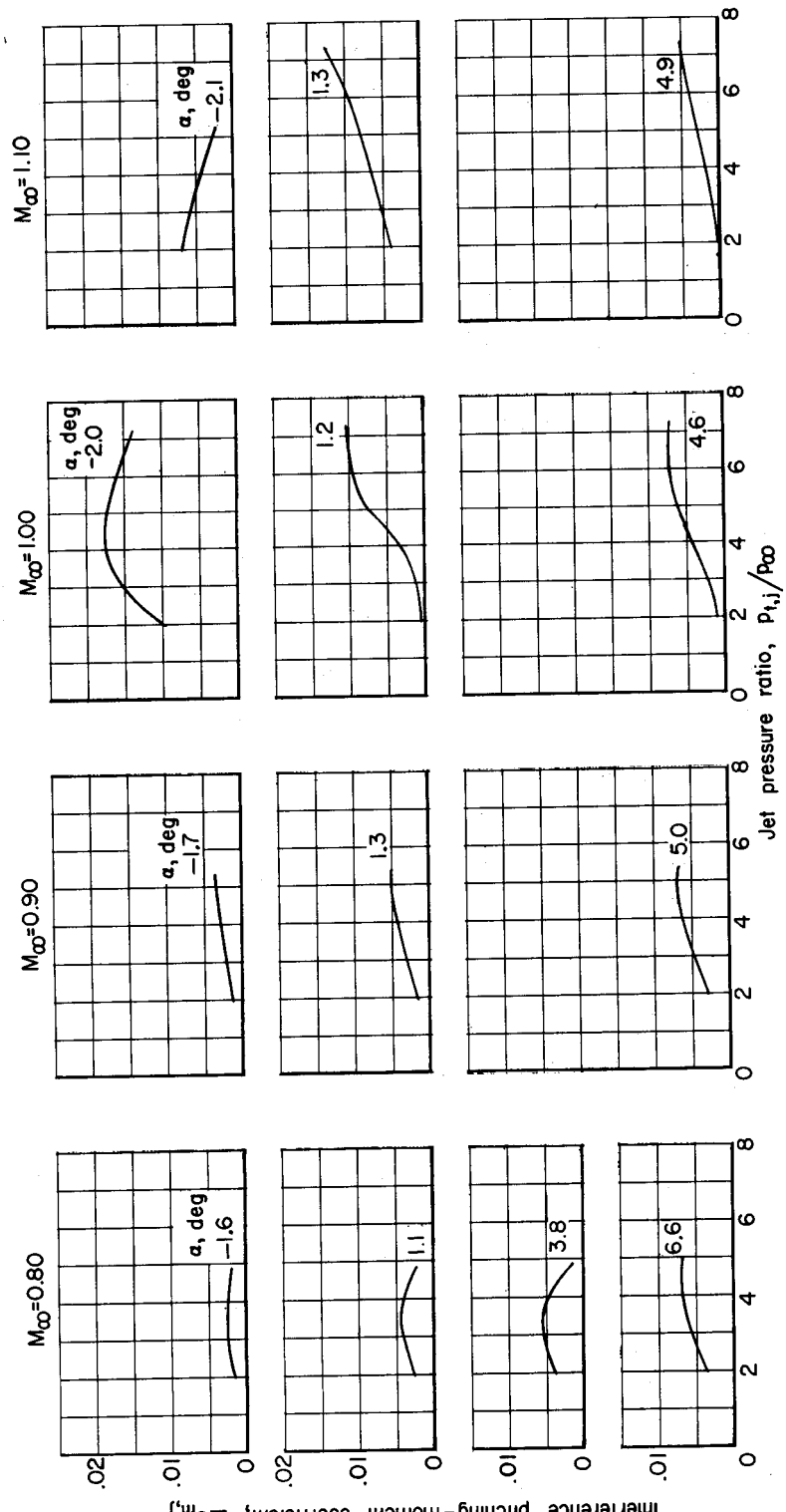

(c) Incremental pitching-moment coefficient due to jet interference.

Figure 12.- Concluded.

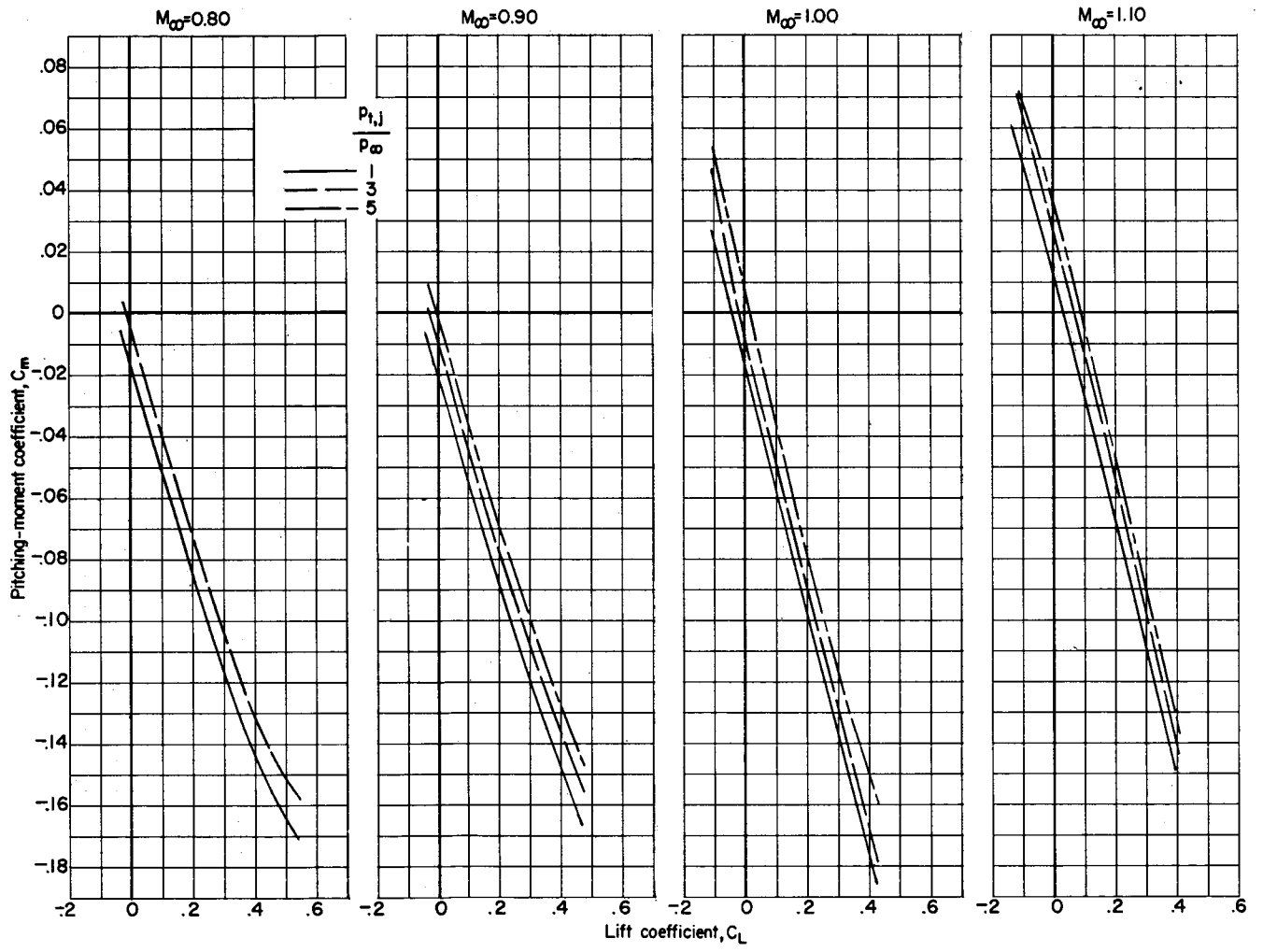

(a) Components of jet thrust included.

Figure 13.- Variation of pitching-moment coefficient with lift coefficient.

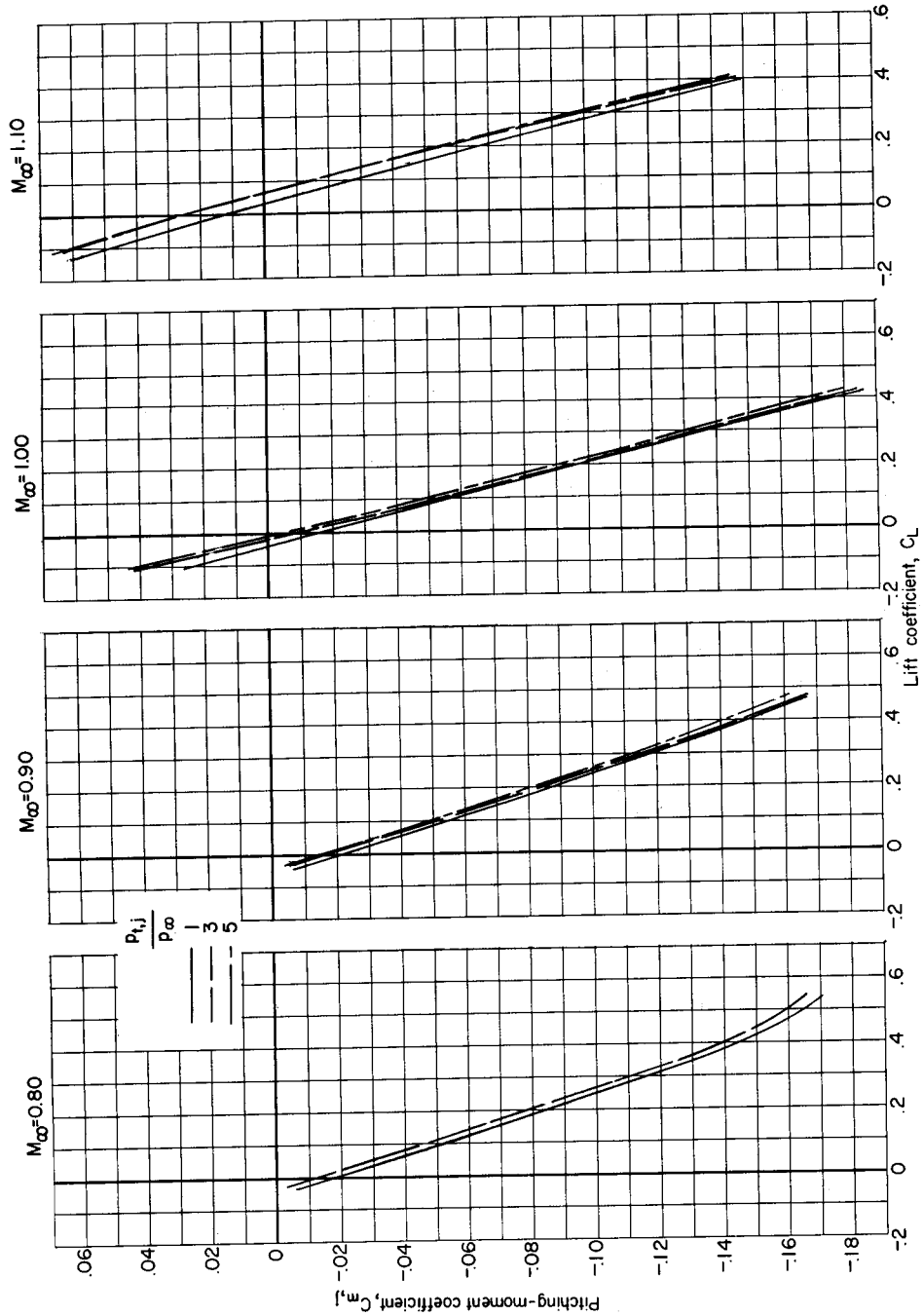

(b) Components of jet thrust removed.

Figure 13.- Concluded.

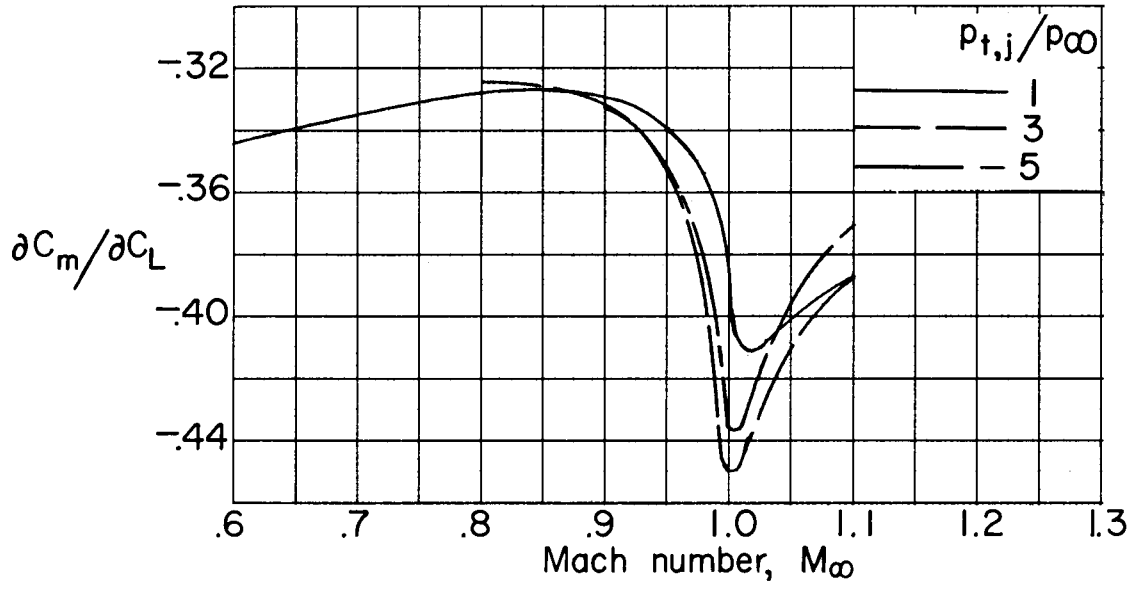

(a) Components of jet thrust included.

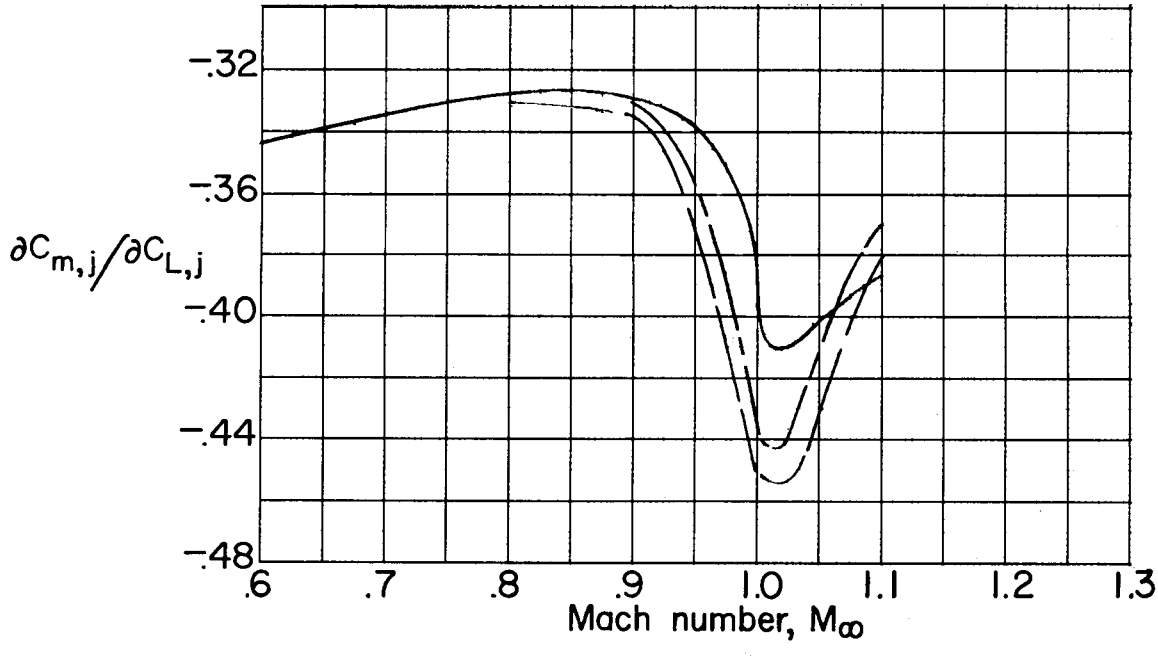

(b) Components of jet thrust removed.

Figure 14.- Effects of jet interference on static longitudinal stability. $\alpha \approx 0^\circ$.

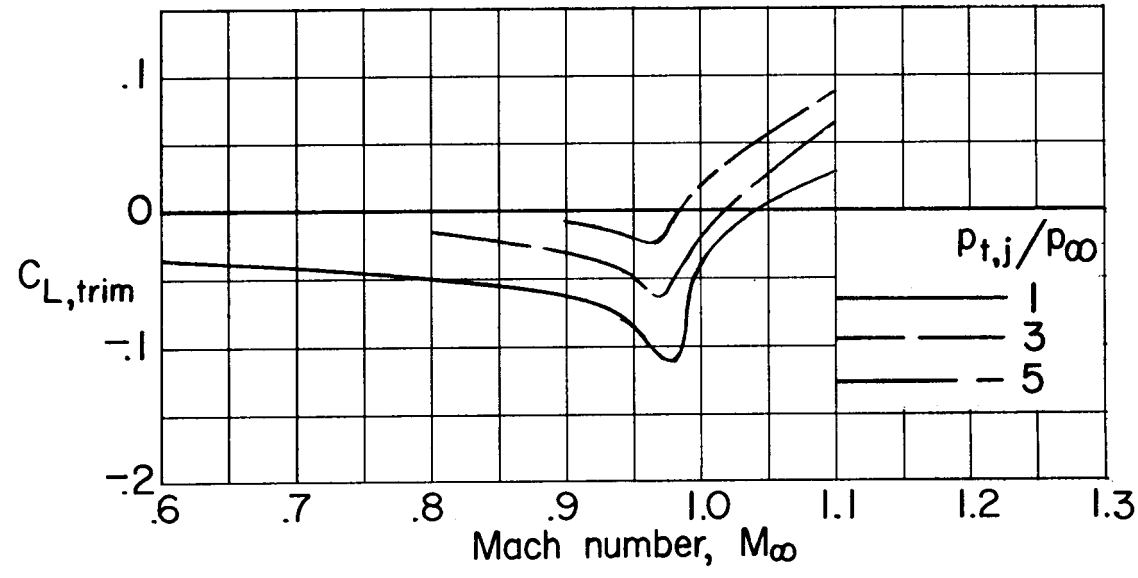

(a) Components of jet thrust included.

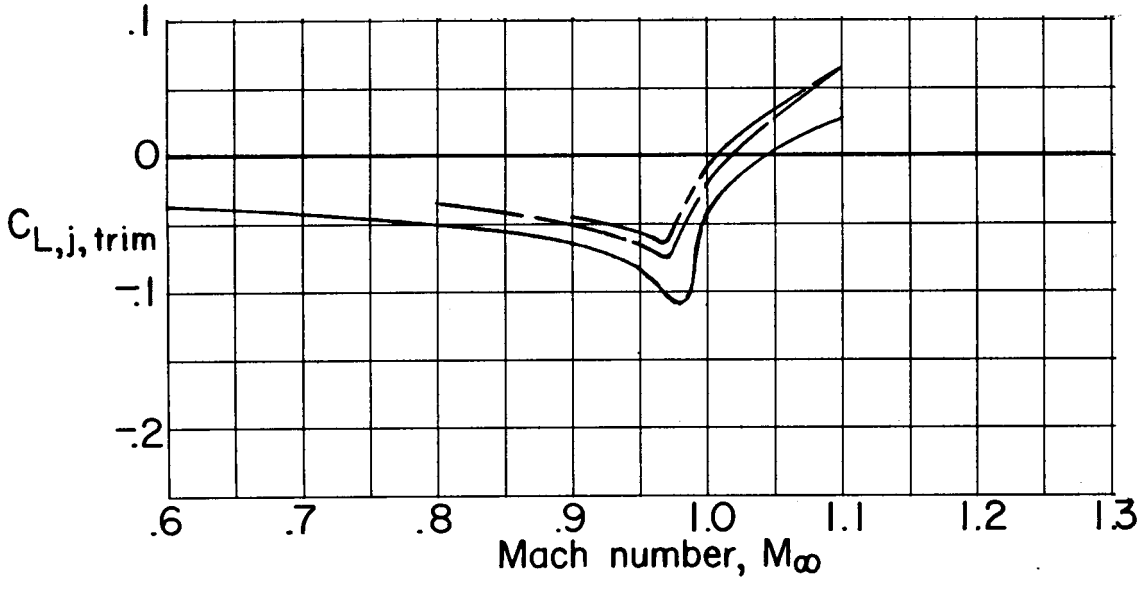

(b) Components of jet thrust removed.

Figure 15.- Effects of jet interference on the lift coefficient required for trim.